

Search for Dijet Resonances in 7 TeV pp Collisions at CMS

The CMS Collaboration
CERN

(Dated: August 30, 2010)

We have used 0.84 pb^{-1} of integrated luminosity from the CMS experiment at the Large Hadron Collider at CERN to search for resonances in the dijet mass spectrum. Upper limits are presented on the product of the resonance cross section, branching ratio into dijets, and acceptance. These generic upper limits are used to exclude at 95% CL intervals of resonance mass (M) for the following specific models of new particles: string resonances for $0.50 < M < 2.10 \text{ TeV}$, excited quarks for $0.50 < M < 1.14 \text{ TeV}$, axigluons and colorons for $0.50 < M < 1.06 \text{ TeV}$, and E_6 diquarks for $0.50 < M < 0.58 \text{ TeV}$.

Within the Standard Model, events with two energetic jets (dijets) arise in proton-proton collisions from parton-parton scattering. The outgoing scattered partons manifest themselves as hadronic jets. The dijet mass spectrum predicted by Quantum Chromodynamics (QCD) falls smoothly and steeply with increasing dijet mass. Many extensions of the Standard Model predict the existence of new massive objects that couple to quarks (q) and gluons (g), and result in resonant structures in the dijet mass spectrum. In this paper we report a search for narrow resonances in the dijet mass spectrum, measured with the Compact Muon Solenoid (CMS) detector [1] at the CERN Large Hadron Collider, at a proton-proton collision energy of $\sqrt{s} = 7 \text{ TeV}$.

In addition to this generic search, we search for manifestations of eight specific models of narrow dijet resonances. First, string resonances are Regge excitations of the quarks and gluons in string theory, with multiple degenerate spin states and quantum numbers [2, 3]. String resonances with mass 2 TeV decay predominantly to $q\bar{q}$ (91%) with small amounts of $g\bar{g}$ (5.5%) and $q\bar{q}$ (3.5%). Second, if quarks are composite particles then excited states are expected, and we search for mass degenerate excited quarks q^* that decay to $q\bar{q}$ [4]. The compositeness scale is set to be equal to the mass of the excited quark. Third, in a model where the symmetry group $SU(3)$ of QCD is replaced by the chiral symmetry $SU(3)_L \times SU(3)_R$, there are axial vector particles called axigluons A , which decay to $q\bar{q}$ [5]. Fourth, the flavor-universal coloron model also embeds the $SU(3)$ of QCD in a larger gauge group, and predicts the presence of a color-octet coloron C , which decays to $q\bar{q}$ [6]. Fifth, grand unified theory based on the E_6 gauge group predicts the presence of scalar diquarks D and D^c , which decay to $\bar{q}\bar{q}$ and $q\bar{q}$ [7]. Sixth, the Randall-Sundrum (RS) model of extra dimensions predicts massive gravitons G , which decay to $q\bar{q}$ and $g\bar{g}$ [8]. For the RS graviton, the value of the dimensionless coupling κ/M_{Pl} is set to 0.1. Seventh and Eighth, models that propose new gauge symmetries often predict new gauge bosons W' and Z' , which decay to $q\bar{q}$ [9]. The W' and Z' resonances are assumed to have standard model couplings and to have fractional widths equal to the corresponding standard model W and

Z bosons.

A detailed description of the CMS experiment can be found elsewhere [1]. The CMS coordinate system has the origin at the center of the detector, the z -axis points along the direction of the counterclockwise beam, with the transverse plane perpendicular to the beam. We define ϕ to be the azimuthal angle, θ to be the polar angle and the pseudorapidity as $\eta \equiv -\ln(\tan[\theta/2])$. The central feature of the CMS apparatus is a superconducting solenoid, of 6 m internal diameter. Within the field volume are the silicon pixel and strip tracker, and the barrel and endcap calorimeters ($|\eta| < 3$): a crystal electromagnetic calorimeter (ECAL) and a brass-scintillator hadronic calorimeter (HCAL). Outside the field volume, in the forward region, there is an iron-quartz fiber hadronic calorimeter ($3 < |\eta| < 5$). The ECAL and HCAL cells are grouped into towers, projecting radially outward from the origin, for triggering purposes and to facilitate the jet reconstruction. In the region $|\eta| < 1.74$ these projective calorimeter towers have segmentation $\Delta\eta = \Delta\phi = 0.087$, and the η and ϕ width progressively increases at higher values of η . The energy in the HCAL and ECAL within each projective tower is summed to find the calorimeter tower energy. Towers with $|\eta| < 1.3$ contain only cells from the barrel calorimeters, towers in the transition region $1.3 < |\eta| < 1.5$ contain a mixture of barrel and endcap cells, and towers in the region $1.5 < |\eta| < 3.0$ contain only cells from the endcap calorimeters.

The integrated luminosity of the selected data sample used for this analysis is $836 \pm 92 \text{ nb}^{-1}$. A single-jet trigger is applied in the online software-level trigger system, known as the High-Level Trigger (HLT), to select an unpre-scaled sample of events for this analysis. A parallel single-jet trigger with a lower p_T threshold is recorded with a prescaling of events for the purpose of computing trigger efficiencies. The trigger efficiency versus dijet mass for this analysis is measured from the data and is greater than 99.5% for dijet masses above 220 GeV.

Jets are reconstructed using the anti- k_T algorithm [11] with a radius parameter $R = 0.7$. The reconstructed jet energy, E , is defined as the scalar sum of the calorimeter tower energies inside the jet. The jet momentum, \vec{p} , is

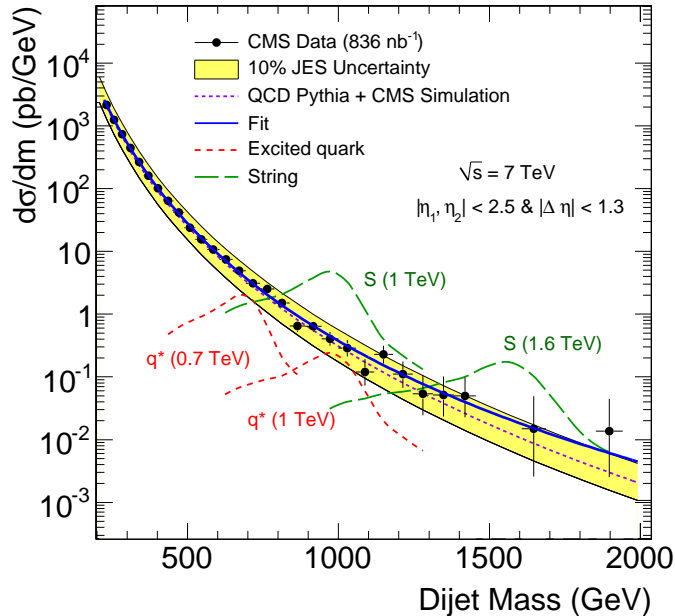


FIG. 1. Measured cross section (points) as a function of dijet mass compared to a smooth fit (solid blue), and to simulations [10] of QCD (dashed blue) excited quark signals (dashed red) and string resonance signals (dashed green) in the CMS detector. The yellow band shows the sensitivity to a 10% systematic uncertainties on the jet energy scale.

the corresponding vector sum of massless towers. The E and \vec{p} of a reconstructed jet are corrected as a function of transverse momentum (p_T) and η for the calorimeter non-linear response and inhomogeneities. The jet energy corrections were determined and validated using Monte Carlo, test beam data, and collision data. [12]

To remove possible instrumental and non-collisional backgrounds in the selected sample the following cuts are made. Events in the sample are required to have a reconstructed primary vertex with $|z| < 15$ cm. Jets are required to have a minimum of 1% of their total energy detected in the ECAL, a minimum multiplicity of 2 calorimeter cells, ECAL or HCAL, and a maximum of 98% of the total energy occurring in a single photodetection device of the hadron calorimeter readout. The jet identification criteria remove less than 0.2% of the events passing the pseudorapidity constraints and dijet mass threshold.

The dijet system is composed of the two jets with the highest p_T in an event (leading jets), and the dijet mass is given by $m = \sqrt{(E_1 + E_2)^2 - (\vec{p}_1 + \vec{p}_2)^2}$. We select events with at least two jets and require that the pseudorapidity separation of the two leading jets, $\Delta\eta = \eta_1 - \eta_2$, satisfies $|\Delta\eta| < 1.3$, and also require that both jets be in the region $|\eta| < 2.5$. These η cuts maximize the search

sensitivity for isotropic decays of dijet resonances in the presence of QCD background.

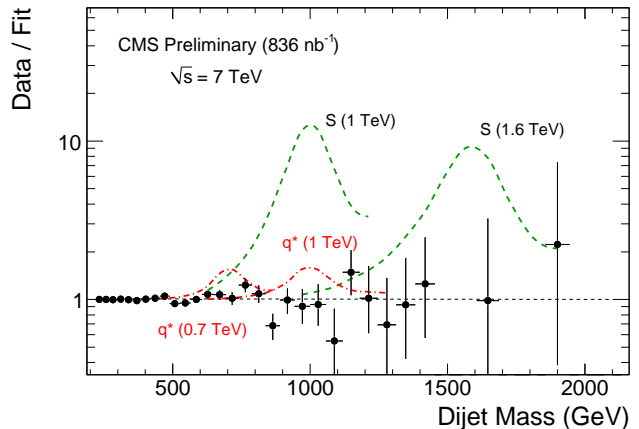


FIG. 2. The ratio between the dijet mass data (points) and a smooth background fit (dashed line) is compared to simulations of excited quark signals (dot-dashed red curves) and string resonance signals (dashed green curves).

In Fig. 1 we present the inclusive dijet mass distribution for $pp \rightarrow 2$ leading jets + X , where X can be anything, including additional jets. We plot the measured differential cross section versus dijet mass in bins approximately equal to the dijet mass resolution. The data is compared to a QCD prediction from PYTHIA [10], which includes a simulation of the CMS detector and the jet energy corrections. The prediction uses CTEQ6 parton distributions [13] and a renormalization scale $\mu = p_T$. The data agrees with the PYTHIA prediction within the systematic uncertainties of the measurement. To test the smoothness of our measured cross section as a function of dijet mass, we fit the data with the parameterization [14]

$$\frac{d\sigma}{dm} = \frac{P0[1 - (m/\sqrt{s}) + P3(m/\sqrt{s})^2]^{P1}}{m^{P2}} \quad (1)$$

with the four parameters $P0$, $P1$, $P2$ and $P3$. In Fig. 1 we show both the data and the fit, which has a χ^2 of 26 for 25 degrees of freedom. In Fig. 2 we show the ratio between the data and the fit. The data is well described by the smooth parameterization and shows no evidence of new particles.

We search for narrow resonances, for which the natural resonance width is negligible compared to the CMS dijet mass resolution. In Figs. 1 and 2 we show the predicted dijet mass distribution for string resonances (S) and excited quarks (q^*) using the PYTHIA Monte Carlo [10] and a CMS detector simulation. The mass resolution has a Gaussian core from jet energy resolution and a long tail towards low mass from QCD radiation. The dijet mass

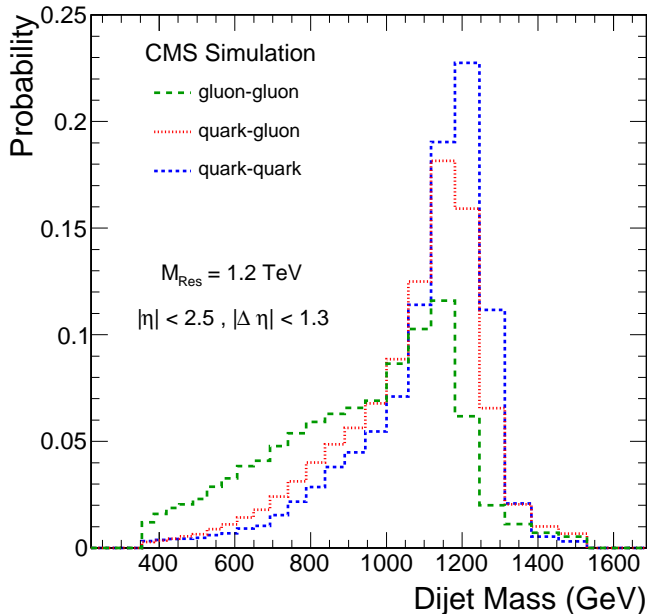


FIG. 3. Simulations of the dijet mass distribution for narrow resonances with mass 1.2 TeV involving parton pairs of type quark-quark (blue), quark-gluon (red), and gluon-gluon (green).

distribution of narrow dijet resonances depends on the type of partons involved in the resonance, because this affects both the amount of radiation and the final state jet response in the CMS detector. In Fig. 3 we show examples of the predicted dijet mass distribution of resonances from three different parton pairings: qq (or $q\bar{q}$) resonances from the process $G \rightarrow q\bar{q}$ [8], qg resonances from the process $G^* \rightarrow qg$ [4], and gg resonances from the process $G \rightarrow gg$ [8]. The width of dijet resonances increases with the number of gluons in the final state, primarily because gluons emit more radiation than quarks. The peak value of the dijet mass for the resonance decreases with the number of final state gluons, primarily due to smaller response of the CMS detector to gluon jets than to quark jets. These resonance shapes are approximately valid for any model of resonance involving these pairs of partons, assuming the models natural half-width ($\Gamma/2$) is small compared to the dijet mass resolution. The dijet mass resolution varies from 10% at 0.5 TeV to 6% at 2.5 TeV for qg resonances. There is no indication of narrow resonances in our data in Fig. 1 or 2

We use the dijet resonance shapes to set separate limits on new particles decaying to the parton pairs qq (or $q\bar{q}$), qg and gg . For setting upper limits, before accounting for systematic uncertainties, we begin with a Bayesian formalism with uniform prior for the cross section. We calculated the posterior probability density as a function

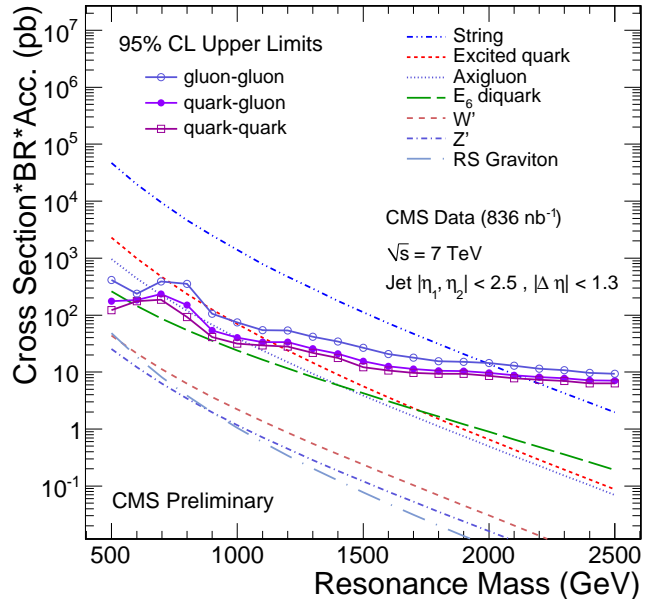


FIG. 4. 95% CL upper limits on the cross section times branching ratio times acceptance for dijet resonances of type gluon-gluon (open circles), quark-gluon (solid circles), and quark-quark (open boxes) compared to theoretical predictions for string resonances [2], excited quarks [4], axigluons [5], colorons [6], E_6 diquarks [7], Randall-Sundrum gravitons [8], and new gauge bosons W' and Z' [9].

of resonance cross section independently at 21 different values of new particle mass from 0.5 to 2.5 TeV in 0.1 TeV steps from which we find initial 95% confidence level upper limits on the cross section, including only statistical uncertainties. The dominant sources of systematic uncertainty were the jet energy scale (10%), the background parameterization choice, the jet resolution (10%) and the luminosity (11%). To incorporate systematic uncertainties, we use an approximate technique which in our application is generally more conservative than a fully Bayesian treatment. The posterior probability density for the cross section is broadened from that without systematic uncertainties by convoluting with a Gaussian systematic uncertainty for each resonance mass [14]. As a result, the cross section limits including systematic uncertainties increase by 16%–47% as a function of resonance mass and type over the corresponding limits derived from statistical uncertainties alone. The generic upper limits at 95% CL on cross section times branching ratio times acceptance for qq , qg and gg resonances are listed in Table I.

In Fig. 4 we compare our upper limits to predictions as a function of resonance mass for specific models. The predictions are lowest order calculations of the cross section times branching ratio times acceptance for dijets satis-

TABLE I. Upper limits at 95% C.L. on cross section times branching ratio times acceptance, listed as a function of new particle mass, for narrow resonances decaying to dijets with partons of type quark-quark (qq), quark-gluon (qg), and gluon-gluon (gg). The limits apply to the kinematic range where both jets have pseudorapidity $|\eta| < 2.5$ and $|\Delta\eta| < 1.3$.

Mass (TeV)	Limit (pb)		
	qq	qg	gg
0.5	123	175	414
0.6	176	185	236
0.7	187	231	375
0.8	93	150	352
0.9	41	53	106
1.0	32	40	75
1.1	29	33	55
1.2	28	34	54
1.3	22	26	42
1.4	18	21	34
1.5	12	15	27
1.6	11	13	21
1.7	9.6	11	18
1.8	9.4	10	16
1.9	9.4	10	15
2.0	8.6	9.7	14
2.1	7.8	8.8	13
2.2	7.3	8.2	11
2.3	7.0	7.8	11
2.4	6.4	7.2	9.7
2.5	6.4	7.1	9.4

fying $|\Delta\eta| < 1.3$ and $|\eta| < 2.5$ with CTEQ6L1 parton distributions [13]. We exclude at 95% C.L. new particles in mass regions for which the theory curve lies above our upper limit for the appropriate pair of partons. For string resonances we use our limits on qg resonances to exclude at 95% C.L. the mass range $0.50 < M(S) < 2.10$ TeV. For comparison, previous cross section upper limits on dijet resonances [15] imply a limit on string resonances of about 1.4 TeV. For excited quarks we use our limits on qg resonances to exclude the mass range $0.50 < M(q^*) < 1.14$ TeV, compared to the previous exclusion of $0.40 < M(q^*) < 1.26$ TeV [16]. For axigluons or colorons we use our limits on qq resonances to exclude the mass range $0.50 < M(A) < 1.06$ TeV, compared to the previous exclusion [15] of $0.12 < M(A) < 1.25$ TeV. For E_6 diquarks we use our limits on qq resonances to exclude the mass range $0.50 < M(D) < 0.58$ TeV, compared to the previous exclusions [15] of $0.29 < M(D) < 0.63$ TeV. The systematic uncertainties included in this analysis re-

duced the excluded upper masses by roughly 0.1 TeV for each type of new particle.

In conclusion, the measured dijet mass spectrum is a smoothly falling distribution which agrees with the predictions of the Standard Model. We see no significant evidence for new particle production, present generic upper limits on the cross section times branching ratio times acceptance that can be applied to any model of dijet resonance, and set specific limits on string resonances, excited quarks, axigluons, flavor universal colorons, and E_6 diquarks.

We thank the technical and administrative staffs at CERN and other CMS Institutes, and acknowledge support from: FMSR (Austria); FNRS and FWO (Belgium); CNPq and FAPERJ (Brazil); MES (Bulgaria); CERN; CAS and NSFC (China); MST (Croatia); University of Cyprus (Cyprus); Academy of Sciences and NICPB (Estonia); Academy of Finland, ME and HIP (Finland); CEA and CNRS/IN2P3 (France); BMBF and DESY (Germany); GSRT (Greece); NKTH (Hungary); DAE and DST (India); IPM (Iran); UCD (Ireland); INFN (Italy); KICOS (Korea); CINVESTAV, CONACYT and UASLP-FAI (Mexico); PAEC (Pakistan); SCSR (Poland); FCT (Portugal); JINR (Armenia, Belarus, Georgia, Ukraine, Uzbekistan); MST and MAE (Russia); MSEP (Serbia); OCT (Spain); ETHZ, PSI, University of Zurich (Switzerland); NSC (Taipei); TUBITAK and TAEK (Turkey); STFC (United Kingdom); DOE and NSF (USA).

-
- [1] R. Adolphi *et al.* (CMS), JINST, **0803**, S08004 (2008).
 - [2] L. A. Anchordoqui *et al.*, Phys. Rev. Lett., **101**, 241803 (2008).
 - [3] S. Cullen, M. Perelstein, and M. E. Peskin, Phys. Rev., **D62**, 055012 (2000).
 - [4] U. Baur, I. Hinchliffe, and D. Zeppenfeld, Int. J. Mod. Phys., **A2**, 1285 (1987).
 - [5] P. H. Frampton and S. L. Glashow, Phys. Lett., **B190**, 157 (1987).
 - [6] E. H. Simmons, Phys. Rev., **D55**, 1678 (1997).
 - [7] J. L. Hewett and T. G. Rizzo, Phys. Rept., **183**, 193 (1989).
 - [8] L. Randall and R. Sundrum, Phys. Rev. Lett., **83**, 4690 (1999).
 - [9] E. Eichten, I. Hinchliffe, K. D. Lane, and C. Quigg, Rev. Mod. Phys., **56**, 579 (1984).
 - [10] T. Sjostrand, L. Lonnblad, and S. Mrenna, (2001), arXiv:hep-ph/0108264.
 - [11] M. Cacciari, G. P. Salam, and G. Soyez, JHEP, **04**, 063 (2008).
 - [12] (2010).
 - [13] J. Pumplin *et al.*, JHEP, **07**, 012 (2002).
 - [14] F. Abe *et al.* (CDF), Phys. Rev., **D55**, 5263 (1997).
 - [15] T. Aaltonen *et al.* (CDF), Phys. Rev., **D79**, 112002 (2009).
 - [16] (2010), arXiv:1008.2461 [hep-ex].